minerals

MDPI

Article

U-Pb Detrital Zircon Ages and Geochemical Features of the Jingxing Formation, (Qamdo Basin, Tibet: Implications): Inferences for the Metallogenic Model of the East Tethys Evaporite

Wenhua Han [1,2,3,*], Haizhou Ma [1,2,*], Weixuan Fang [4], Huaide Cheng [1,2], Yongshou Li [1,2], Binkai Li [1,2], Weiliang Miao [1,2] and Qinyu Hai [1,2]

1 Key Laboratory of Comprehensive and Highly Efficient Utilization of Salt Lake Resources, Qinghai Institute of Salt Lakes, Chinese Academy of Sciences, Xining 810008, China; chenghuaide@isl.ac.cn (H.C.); yongshouli@isl.ac.cn (Y.L.); libk@isl.ac.cn (B.L.); weiliangm@isl.ac.cn (W.M.); hqy@isl.ac.cn (Q.H.)
2 Qinghai Provincial Key Laboratory of Geology and Environment of Salt Lakes, Xining 810008, China
3 University of Chinese Academy of Sciences, Beijing 100049, China
4 China Non-Ferrous Metals Resource Geological Survey, Beijing 100012, China; fangwuxuan@tom.com
* Correspondence: hanwenhua@isl.ac.cn (W.H.); haizhou@isl.ac.cn (H.M.)

check for updates

Citation: Han, W.; Ma, H.; Fang, W.; Cheng, H.; Li, Y.; Li, B.; Miao, W.; Hai, Q. U-Pb Detrital Zircon Ages and Geochemical Features of the Jingxing Formation, (Qamdo Basin, Tibet: Implications): Inferences for the Metallogenic Model of the East Tethys Evaporite. *Minerals* **2021**, *11*, 745. https://doi.org/10.3390/min11070745

Academic Editor: Krzysztof Bukowski

Received: 22 May 2021
Accepted: 30 June 2021
Published: 9 July 2021

Abstract: Qamdo basin is located between the suture zone of Jinsha River (Ailao Mountains) and that of Ban Gong Lake (Nujiang) in the eastern Tethys. Part of the Jingxing Formation is deposited in the southwest of the basin. In this study, two profiles were investigated from the north and south of Qamdo basin. The characteristics of detrital zircon LA-ICP-MS U-Pb age, and the main and trace elements of sandstone were analyzed. The characteristics of major and trace elements showed that the tectonic setting of the study area is mainly composed of a relatively stable active continental margin and a passive continental margin, showing characteristics of a continental island arc. The weathering degree of Jingxing Formation in the Qamdo area is lower than that in the Lanping-Simao area, which may be closer to the origin. The age distribution characteristics of detrital zircon grains indicate that the Qiangtang Block, Youjiang basin, and Yangtze area jointly constitute the provenance of the Qamdo-Lanping-Simao basin. Both basins may be part of a large marine basin with unified water conservancy connection before evaporite deposition. Metamorphic seawater from the Qamdo basin may migrate to the Lanping-Simao basin and even the Khorat basin, where evaporite was deposited.

Keywords: Jingxing Formation; provenance; geochemistry; U-Pb detrital zircon age; Qamdo basin

1. Introduction

The formation and evolution of the Tethys, which encompasses the five current continents of Europe, Asia, Africa, South America, and North America, exerted an important influence on the global structure. The Tethys tectonic area is rich in salt resources, and reaches from northern to eastern Europe, north Africa, west Asia, and central Asia to China [1,2]. Qiangtang basin is located in the northern part of the Qinghai-Tibet Plateau and the eastern part of the Tethys-Himalayan tectonic domain (Figure 1). It is the largest Meso-Cenozoic sedimentary basin in the Qinghai-Tibet Plateau [3–6]. In recent years, a giant Jurassic potash deposit has been discovered in the Karakum basin in the north margin of the Qiangtang basin [7–10]. Several Jurassic gypsum beds and gypsum mound outcrops at different scales were also found in the northern Qiangtang basin, especially many salt springs in the northern Qiangtang basin, whose water composition reached the deposition index of magnesium sulfate, which was close to that of potassium salt. Qiangtang basin has better salt-forming geological conditions and potassium-forming potential [11,12]. Qamdo basin is located in the east of Qiangtang basin. This area has an

abundance of salt spring water, gypsum salt, dolomite, and magnesite. Qamdo basin is connected with Lanping-Simao basin in the south, and extends to Laos, Thailand, and Nakhon Lat plateau in the south, which together constitute a large rift basin system. The Mengye jing potash deposit in Jiangcheng, Lanping-Simao basin is the only ancient solid potash deposit of mining value in China. Its ore-bearing stratum is the Mengye jing Formation, which, along with rock salts and clastic rocks, is part of the Mengye jing Formation [13]. A number of scholars inferred that the sedimentary age of the Mengye jing Formation was the late Early Cretaceous by studying the tuff interlayer (SHRIMP dating), palynology, and high-precision paleomagnetism of the formation [14,15]. *Microaenator chagyabi*, *Asiatosaurus kwangshiensis*, *Monkonosaurus lawulacus*, and other dinosaur fossils have been found in the Jingxing Formation of Qamdo. The sedimentary age of Jingxing Formation in Qamdo area may be the Early Cretaceous, and the lithologic assemblage and paleontological fossils of Jingxing Formation in the study area are basically identical to those of Jingxing Formation in the Lanping-Simao area [16]. Wang and Li studied the provenance of detrital zircon grains from Mengye jing Formation and Baishahe Formation in the Simao area of Lanping, and concluded that Qiangtang Block, Ailaoshan tectonic belt, Yangtze, and other areas jointly constituted the provenance of the Lanping-Simao basin [17,18]. Geochemistry and sulfur isotopic characteristics of anhydrite indicate that the evaporite deposits in the Qamdo-Lanping-Simao basin have marine facies genesis [18–20]. Hite and Japalcaster (1979) inferred that the Khorat area (such as the ocean) has a water conservancy contact to the southwest [21]. Wang (2014) studied the Lanping area and suggested that the formation of evaporite was related to the transgression of the Neo-Tethys Ocean in the middle Cretaceous [19]. Wang further pointed out that the Lanping-Simao-Vientiane-Khorat basin is in the transgression period for unified large evaporation basin systems, which are interconnected [17]. Recent studies have shown that large-scale evaporites, developed in the Qamdo-Lanping-Simao basin, were concentrated metamorphic seawater after the Neo-Tetyan Ocean seawater passed through the North Qiangtang confined sea and entered the basins of the salt-forming zone. This is a concentrated metamorphic migration model of multi-stage basin seawater into salt-forming potassium [18]. However, direct evidence for the provenance of Early Cretaceous strata in the Qamdo-Lanping-Simao basin is still lacking. Therefore, it is of great significance to study the provenance of the Early Cretaceous Jingxing Formation in Qamdo basin.

Zircon grains are highly refractory during cycles of geologic history. Over the last 20 years, hundreds of published studies using detrital zircon grains indicate the increasing success in evaluations of provenance and paleogeography and developing tectonic reconstructions [22,23]. U-Pb ages of detrital zircon grains can therefore effectively constrain the sources and origins of detrital zircon grains in sedimentary rocks [24,25]. The whole-rock geochemistry of sandstones can also be used for provenance analysis [26,27]. In this study, an integrated approach of whole-rock geochemistry and detrital zircon U-Pb was used. The obtained data are used to constrain the sedimentary provenance of the Late Cretaceous Jingxing Formation and study the relationship between Jingxing Formation and Meyejing Formation. New evidence for the mineralization model of evaporite deposit is put forward.

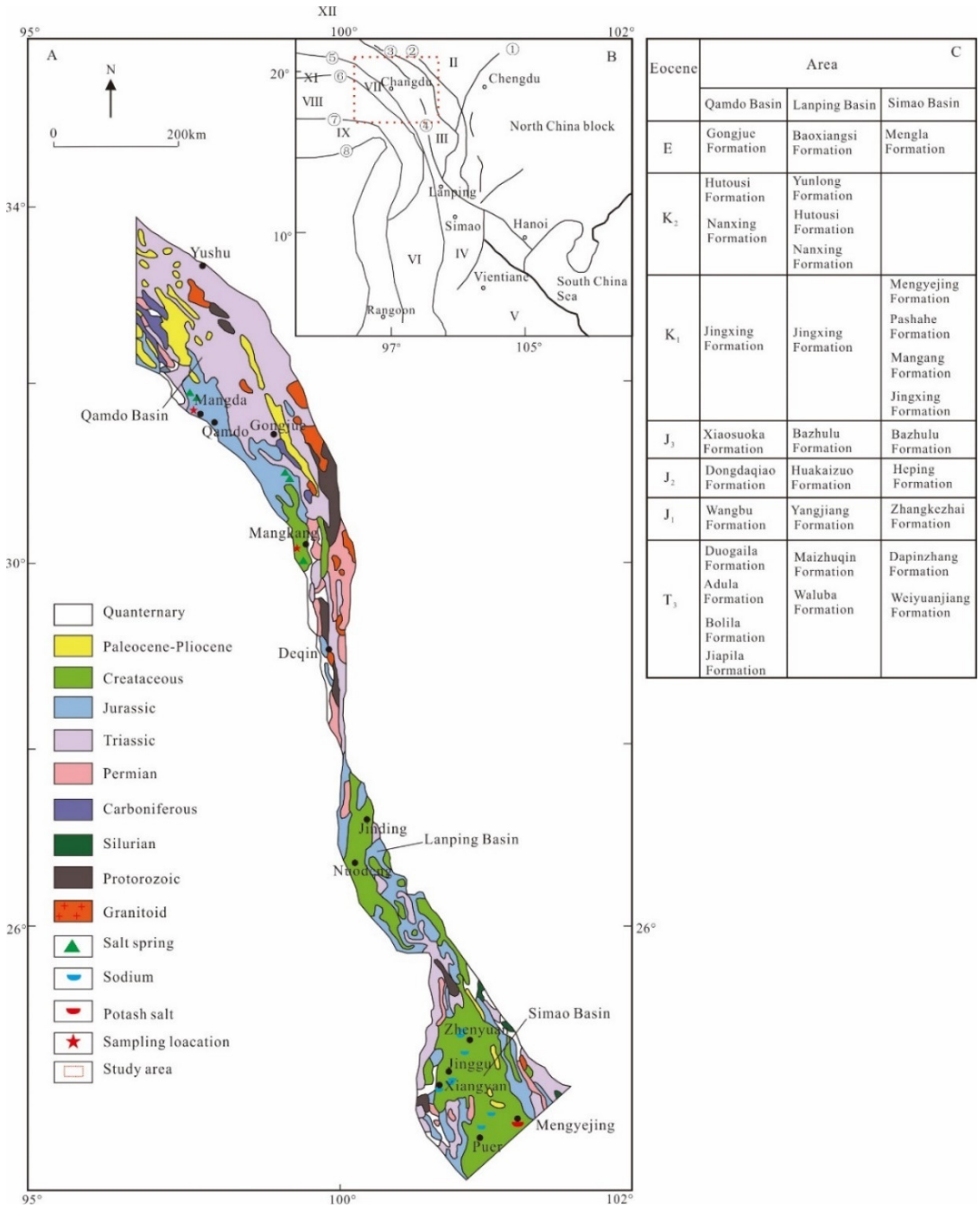

Figure 1. (**A**) geological map (modified after Song et al., 2011 [28]; salt springs after Qin et al., 2017 [29]; salts after Wang et al., 2018 [30]); (**B**) Schematic tectonic map of Qamdo: Notes: I: North China Block; II: Songpan-Ganzi Block; III: Yidun Arc Terrane; IV: Qamdo-Simao Block; V: Indochina Block; VI: Baoshan Block; VII: Qiangtang Block; VIII: Gangdisi Arc; IX: Himalayan Block; X: Himalayan Front Thrust Belt; XI: Qinghai-Tibet Plateau; ① Longmenshan Fault Zone; ② Daofu-Luhuo Fault Zone; ③ Garze-Litang Suture Zone; ④ Jinshajiang-Ailaoshan Suture Zone; ⑤ Shuanghu-Lancangjiang Suture Zone; ⑥ Bangong-Nujiang suture Zone; ⑦ Yarlung-Zangbo Suture Zone; ⑧ Himalayan Thrust Belt (modified after Hou et al., 1996 [31]); (**C**) Stratigraphic column (modified after Miao [32]).

2. Geological Setting

Qamdo Basin is located at 96°30′–99°30′ E and 29°00′–31°40′ N of the eastern Qinghai-Tibet Plateau, with NNW-SSE direction (Figure 1), covering an area of about 4.8 × 10^4 km^2. The Qamdo basin developed in the Qiangtang, Qamdo-Simao Block, and the Jinshajiang-Ailaoshan suture zone is in the northeast, which is characterized by the final extinction

of Jinshajiang-Ailaoshan in the Late Triassic and the collision of the Qamdo block and Songpan-Ganzi block since the Late Triassic. In the southwest, the Bangong-Nujiang Suture Zone closed with the Bangonglake-Nujiang basin in the middle and late middle Jurassic [33–35]. The tectonics of Qamdo area belong to the eastern section of the East Tethys tectonic domain, which is an arc-continental collision orogenic belt that formed since the Late Paleozoic. Since the Paleozoic, three major tectonic system changes have occurred, namely, the Late Paleozoic to Middle Triassic multi-arc basin to orogenic belt transition, the Late Triassic to Cretaceous basin-mountain transition, and the Cenozoic large-scale intracontinental tectonic convergence [36–40].

The strata exposed in Qamdo basin are mainly Pre-Ordovician, Ordovician, Upper Paleozoic, Mesozoic, and Cenozoic. The Mesozoic middle and lower Triassic strata are mainly distributed in the east of the basin, and in the narrow zone from the south of Yushu to the area of Mangkang. The distribution in the basin is sporadic. These strata are purplish red, grayish green, and gray medium thin layers of sandstone and shale interbedded with volcanic rocks [41]. The Mesozoic strata in the southern part of the basin are relatively well preserved in the Mangkang area. The denudation in the northern Qamdo area is relatively large, and the Upper Triassic-Jurassic strata are only exposed in Mangda Town. The main Triassic formations are Jiapila Formation (T_3j), Bolilia Formation (T_3b), Adula Formation (T_3a), and Duogaila Formation (T_3d). The Jiapila Formation is interbedded with purplish red conglomerate, sandstone, and shale. The bottom is unconformable above the Upper Permian strata, and the top is conformable covered with limestone of Bolila Formation. Bolila Formation is a set of carbonate formations with the bottom integrated over Jiapila Formation. Bolila Formation is composed of light gray medium-thick stratified limestone, micritic limestone, nodular limestone, and bioclastic limestone, and its distribution is stable. Adula Formation is composed of gray and dark gray thin-bedded to intermediate mudstone, siltstone interbedded with feldspar quartz sandstone, and coal lines, containing plant fragments. Duogaila Formation is a set of coastal and lagoonal facies deposited with abundant plant fossils and a small amount of brackish bicrustal fossils, which are interbedded with grey-black thin-bedded sandstones and shales. Triassic strata present a set of gypsum deposits. The Jurassic is mainly composed of fluvio-lacustrine clastic rock deposits, interbedded with marine strata, generally consisting of a set of red and purplish red strata. Together with the Cretaceous system, these constitute the so-called "red basin" of Qamdo basin, with a main distribution in Qamdo-Mangkang. Jurassic strata include Wangbu Formation (J_1w), Dongdaqiao Formation (J_2d), and Xiaosuoka Formation (J_3x). Jurassic lithology in Qamdo basin is mainly composed of purplish red sand and argillaceous rocks, and deposits of thick layers of gypsum ore [42]. Cretaceous strata include the Jingxing Formation (K_1j), Nanxin Formation (K_2n), and Hutousi Formation (K_2h), which are in parallel unconformable contact with underlying strata. Nanxin Formation consists of a set of purplish red sandstone, complex lithic conglomerate, and conglomerate. It is a fluvial facies deposit, and the strata only outcropped in the north of Mangkang area. Hutousi Formation is a large set of cross-bedding with thick bedded sandstone and purple mudstone. This belongs to river and arid hot salt water lacustrine deposits, and few outcrops can be found in the study area. The strata of Jingxing Formation (K_1j) are local outcrops in Jiangda County and Mangkang County, and are the target strata of this study. The lithology is mainly composed of purplish red feldaceous conglomerate, mud-bearing coarse sandstone with color, and silty mudstone, which belongs to fluvio-lacustrine deposits. The strata are integrated on the Xiaosuoka Formation (J_3x) [16]. On the whole, the area of Cretaceous strata outcrops in Qamdo basin is small; therefore, the research foundation of Cretaceous strata in this area is relatively weak.

3. Materials and Methods

The geochemical analysis of the major and trace elements of the samples was completed in the laboratory of the Beijing Research Institute of Uranium Geology, Beijing, China. The working environment temperature was 20 °C and humidity was 40%. The major ele-

ments were tested and analyzed by X-ray fluorescence spectrometry on a Panaco AXIOS X-ray fluorescence spectrometer (Malvern Panalytical, Malvern, UK), with an analysis error of less than 5%. Trace elements were measured using a Finnigan MAT (Thermo Fisher Scientific, Waltham, MA, USA) high-resolution inductively coupled plasma mass spectrometer (ICP-MS). The details of this analytical procedure have been described by Cullen et al. [43]. The accuracy of the analyses was better than 2.5%.

Samples for this study were collected from the section in Mangda Town and west of Mangkang County, where the Mesozoic strata of Jingxing Formation are well exposed. A total of 23 sandstone samples were collected from two sections of the Jingxing Formation, and the contents of major elements and rock slices of samples were studied. Two samples from the Jingxing Formation were collected from Mangda and Mangkang areas and were subjected to U-Pb geochronology by the State Key Laboratory of Continental Dynamics, Northwest University, Xian, China. Each sample was selected from fresh sandstones. Zircon grains were separated using conventional heavy liquid and magnetic techniques and were purified by handpicking under a binocular microscope. A total of 204 representative grains of each sample were mounted in a 25-mm epoxy-resin mount and then polished and coated with gold film. Cathodoluminescence images of zircon grains were used to assess the internal growth structures of the zircon grains. The best zircon particles without inclusions and cracks were selected for LA-ICP-MS test. The analytical instrument was an Agilent 7700X ICP-MS (MicroLas, Göttingen, Germany) and the matching GeoLas2005 laser erosion system was used. During the experiment, He was used as carrier gas, and the diameter of the laser beam spot was 25 μm. Zircon 91500 was used as external standard for U-Pb dating, and NIST SRM 610 was used as external standard for both the U and Th contents. The zircon U-Pb age concordia and probability density plots were drawn using the Isoplot (version 3.0) software of Ludwig and Hou [44,45].

4. Results

4.1. Petrography

The lithology of the Cretaceous Jingxing Formation in the study area is mainly medium-fine feldspar lithic sandstone and siltstone. Its structural components are characterized by fine particle size of 0.06–0.5 mm, pore type of cementation, good to medium sorting, sub-angular grinding degree, and moderate weathering degree, indicating relatively weak hydrodynamic conditions during deposition. The contents of quartz, feldspar, and lithic fragments in the detrital composition are 51%, 14%, and 35%, respectively. The cement content is 3–6%. Feldspar is widely distributed in the study area (Figure 2), mainly as plagioclase, potassium feldspar, sericited and kaolinited plagioclase are common, resulting in a dirty surface. Occasionally, the plagioclase secondary increase phenomenon can be observed, increasing the side for albitization. Feldspar is often selectively dissolved and metasomatized by carbonate along cleavage fractures. The higher the content of feldspar and lithic fragments, the lower the compositional maturity of the rock. The content of lithic fragments in this study area is relatively high, and their types are complex and diverse. The volcanic rock lithic fragment in magmatic rocks are the main fragments (Figure 2B,D), and contain a small amount of granite, metamorphic quartzite, micritic limestone, and siliceous rocks. Volcanic rock lithic fragment is dominated by acid extrusive rock lithic fragment, which is characterized by porphyritic structure or the lack thereof. The phenocryst is quartz or transfeldspar, its matrix has either a felsic structure, radiating spherular structure, or microscopic cryptocrystalline structure, and the structures are massive, occasionally showing a flow structure and felsic mineral composition. The granite lithic fragment has a semi-idiomorphic granular structure (i.e., granitic structure) and massive structure. The main mineral components are quartz, potassium feldspar, and plagioclase. Metamorphic quartzite is generally composed of two or more quartz particles, which are colorless and transparent. Quartz particles are inlaid and contacted with each other, and show clear wavy (or banded) extinction. Micritic limestone lithic fragment generally has a micritic structure, mineral composition of micritic calcite, with an extremely unstable

nature, similar to near provenance lithic fragment. The cuttings of siliceous rock are colorless and transparent, and show smooth surface, small grain structure, or radial spherular structure, and a mineral composition of cryptocrystalline quartz.

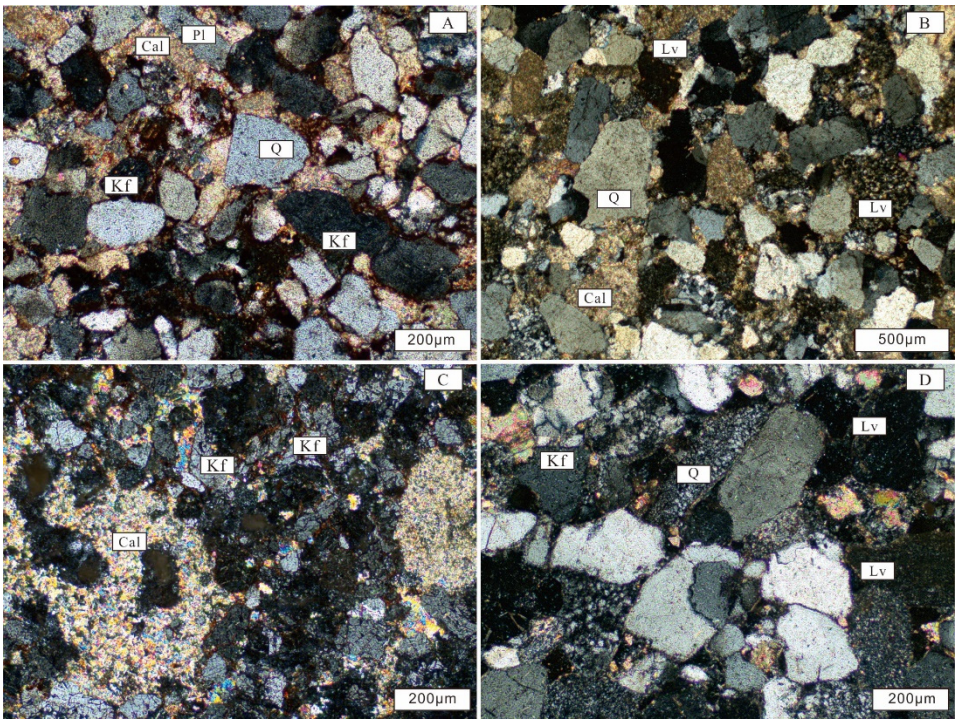

Figure 2. Photomicrographs of typical lithics in sandstones of the Jingxin Formation under cross-polarized light. (**A**,**B**), sample MP4 in section of Mangda. (**C**,**D**), sample MK11 in section of Mangkang. Abbreviations: Q, quartz; Cal, calcite; Pl, Plagioclase; Kf, K-Feldspar; Lv, volcanic rock fragment.

4.2. Whole Rock Geochemistry

The results of the major elements from the Jingxing Formation sandstone in the Qamdo Basin show that the data of the major elements from both sections are basically identical, and the variation range is weak. The results of the elements data are given in Supplementary Data Table S1. According to the data of both sections, SiO_2 ranges from 54.68% to 79.72%, with an average of 66.42% (n = 23). This is consistent with the average value of the upper crust (65.89 wt.%) [46]. Al_2O_3 ranges from 3.80% to 20.09%, with an average of 11.86%, which is lower than the average of the ucc (15.17 wt.%) [46]. $Fe_2O_3^T$ ranges from 1.13% to 8.12% with an average of 4.38%; MgO ranges from 0.31% to 2.78% with an average of 1.74%, Na_2O ranges from 0.06% to 1.51% with an average of 0.99%; K_2O ranges from 0.46% to 4.82% with an average of 2.56%; CaO ranges from 0.49% to 9.00% with an average of 4.29%; TiO_2 ranges from 0.20% to 0.86% with an average of 0.60%; MnO ranges from 0.02% to 0.16% with an average of 0.07%; and P_2O_5 ranges from 0.05% to 0.18% with an average of 0.13%. Geochemistry classification diagrams (Figure 3A) show that samples from the Jingxing Formation of both the Mangda section and Mangkang section are located in the area of arkose sandstone and lithic greywacke. These show a low number of samples in sublithic sandstone, and have a tendency to transform to subarkose sandstone. In the Na_2O-K_2O diagram (Figure 3B), a large part of samples from both sections fall into the quartz rich and quartz-intermediate categories of subarkose sandstone.

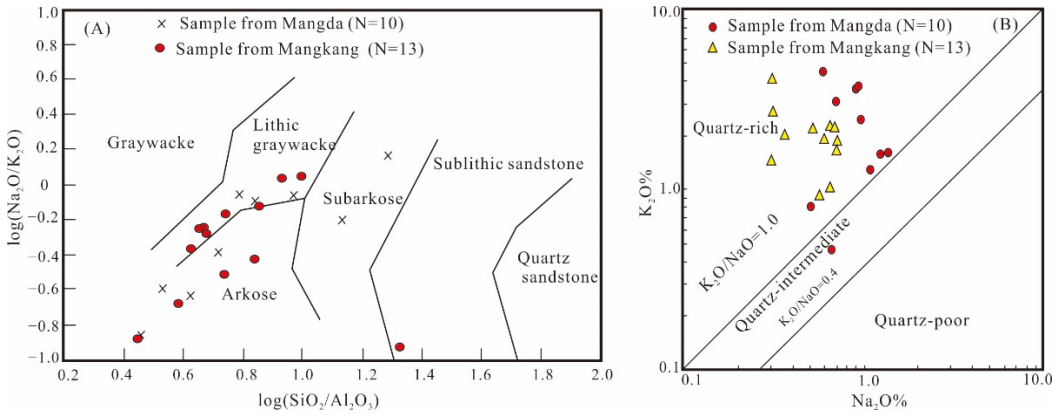

Figure 3. Geochemistry classification diagrams of sandstones of the Jinxing Formation in Qamdo basin (**A**, after Pettijohn et al., 1972 [47]; **B**, after Asiedu et al., 2000 [48]).

In the process of magma or fluid evolution, compatible elements (e.g., Ni and Co) mostly enter the mineral phase or the residual phase, while incompatible elements are more inclined to enter the melt phase. Therefore, in contrast to the major elements, trace elements record different geological activities in a unique way [46]. As shown in Figure 4A, all samples have similar chondrite normalized rare earth element (REE) profiles. The normalized distribution patterns of REEs in chondrites show that light REE are enriched, while the contents of heavy REE are low. The total amount of REE (ΣREE) ranges between 66.48 μg/g and 243.25 μg/g, with an average value of 145.2 μg/g. The total amount of light rare earth elements (ΣLREE) ranges from 59.89 μg/g to 223.0 μg/g, with an average value of 131.14 μg/g. The content of heavy rare earth elements (ΣHREE) ranges from 60.59 μg/g to 20.61 μg/g, with an average value of 14.07 μg/g. The ratio of LHREE to heavy rare earth elements (LHREE/HREE) ranges from 7.23 μg/g to 11.01 μg/g with an average of 9.23 μg/g. The Eu element has an obvious negative anomaly. Figure 4B shows that the Jingxing Formation sandstone in Qamdo area has low contents of high field strength elements such as K, Nb, Sr, P, and Ti.

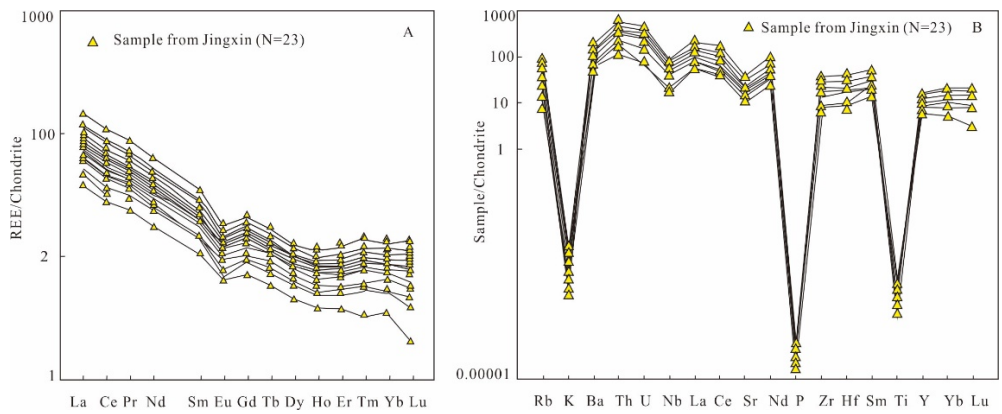

Figure 4. (**A**) Chondrite-normalized rare earth element (REE) patterns of sandstones of the Jingxing Formation (after Taylor and McLennan 1985 [46]). (**B**) Chondrite-normalized trace element spider diagram of the sandstones of Jingxing Formation (after Taylor and McLennan 1985 [46]).

4.3. U-Pb Geochronology

In this study, 102 detrital zircon grains from sample MP4 were tested, which is located in the Mangda Town. Among them, three did not meet the requirements of concordance (concordance <90% and >110%), and the remaining 99 samples met the research requirements. The effective data accounted for about 97% of the data. The U-Pb data are given in Supplementary Data Table S2. The interpreted ages are based on the $^{206}Pb/^{238}U$ for <1000 Ma grains and on the $^{207}Pb/^{206}Pb$ for >1000 Ma grains [49]. In sample MK11, which was

located in Mangkang County, 102 detrital zircon grains were tested, two of which also failed to meet the requirements of concordant degree, and the remaining 100 met the research requirements. The effective age data accounts for about 98% of the overall analyzed data (Table S2). The U-Pb data for each sample are presented in concordia diagrams and relative probability plots (Figure 5). These data are discussed together in view of the two samples with similar detrital age compositions according to the age distribution characteristics. Based on the age distribution characteristics of the two samples from Jingxing Formation, the minimum age is 195.4 Ma, the youngest cluster of ages ranges within 194–218 Ma, the peak age for this age group is 220 Ma, and the maximum age is 2734.2 Ma. The age of two samples is mainly concentrated in 198–608 Ma, 721–1006 Ma, and 1694–2082 Ma. In the detrital zircon grain age spectrum diagram, the ages of coarse sandstone in the Jingxing Formation mainly showed three peaks of 450 Ma and 1870 Ma.

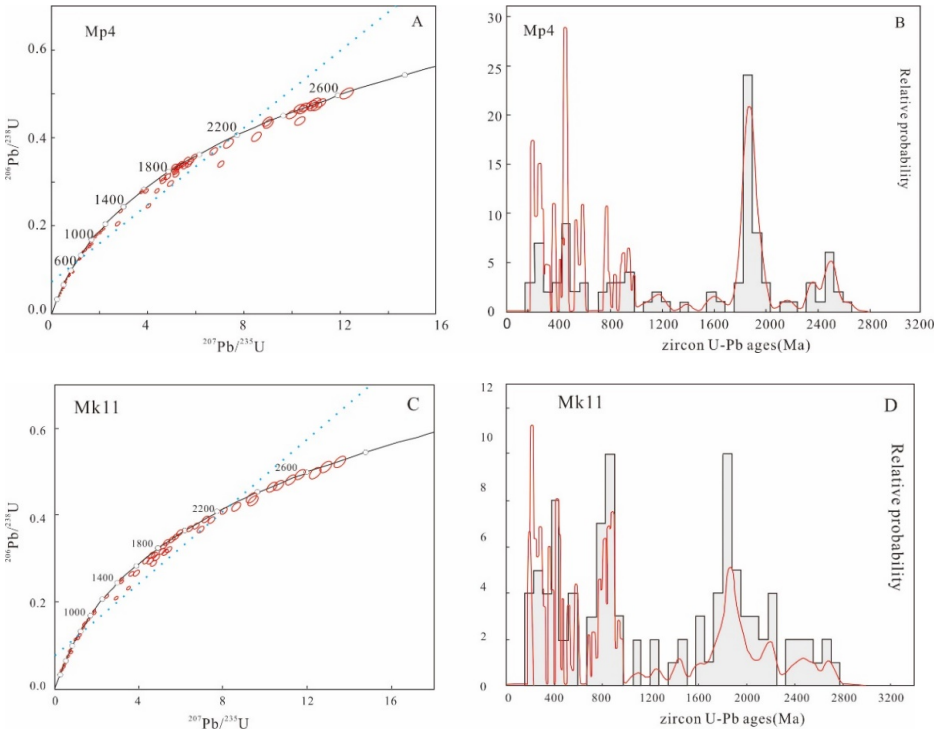

Figure 5. U-Pb concordia diagrams and age probability plots for samples of Jingxing at Qamdo Basin. (**A**,**B**) Sample MP4 of Mangda section. (**C**,**D**) Sample MK11 of Mangkang section.

The Cathodoluminescence (CL) images of representative zircon grains and the spot ages are shown in Figure 6. The morphologies of these zircon grains vary widely from prismatic crystals to oval shapes. These zircon grains can be divided into two groups: (1) euhedral, subhedral, anhedral, elongated, and zoned grains were assigned to the 'idiomorphic' group, while (2) rounded and subrounded zircon grains constitute the 'rounded' group. Several grains were broken and may have been damaged during transport. Other grains are subrounded or have rounded corners. This rounding of grains suggests prolonged transport or multiple cycles of transport, whereas euhedral grains typically suggest short transport distances. Most zircon grains have well-developed oscillating zoning or striped zoning structures, showing magmatic origin under CL. Other grains have internal structures that indicate a typical metamorphic origin, i.e., unzoned, weakly zoned, cloudy-zoned, sector-zoned, planar-zoned, and patched-zoned [50]. Zircon grains of magmatic origin generally have a high Th/U value (usually exceeding 0.4), while metamorphic zircon grains generally have a Th/U ratio below 0.1. Fast-growing metamorphic zircon grains have relatively high Th/U ratios, and incomplete recrystallized zircon grains may also have relatively high Th/U ratios [51,52]. A number of metamorphic zircon grains even

have a Th/U ratio of 0.7 [53]. About 63% of the zircon grains from the Mangda section have Th/U ratios exceeding 0.4, and about 5% of the zircon grains have Th/U ratios less than 0.1%. About 66% of the zircon grains from the Mangkang section have Th/U ratios exceeding 0.4, and about 3% have Th/U ratios below 0.1%. Based on the Th/U ratios of both sections, most of the zircon grains are magmatic zircon grains. Cathodoluminescence images of zircon grains show a cloudy structure with Th/U ratio below 0.1, which may be the product of metamorphism.

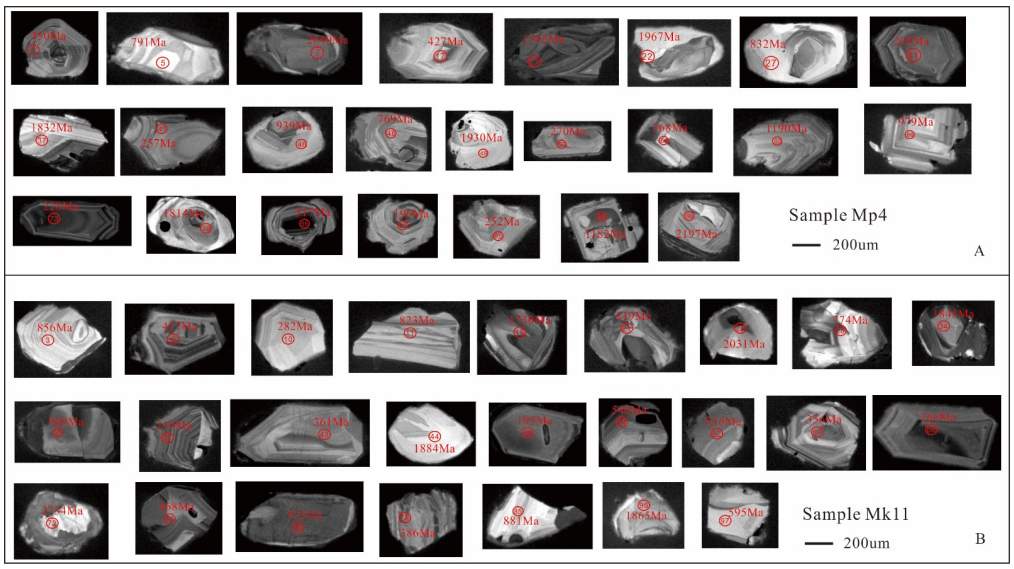

Figure 6. Representative cathodoluminescence images for detrital zircon grains of sandstone samples from Qamdo. The laser spots and corresponding ages are marked. (**A**) Sample MP4 of Mangda section. (**B**) Sample MK11 of Mangkang section.

5. Discussion

5.1. Source Area Weathering and Sediment Recycling

The contents of unstable oxides (e.g., CaO, Na_2O, K_2O, and MgO) and relatively stable oxides (e.g., Al_2O_3, ZrO_2, and TiO_2) contained in the parent rocks in the region of origin will change significantly after weathering or chemical metasomatism during diagenesis [54]. Wedepohl [55] suggested that the upper crust is composed of about 21% quartz, 41% plagioclase, and 21% potassium feldspar; therefore, feldspar minerals play a very important role in the weathering process of the upper crust. The weathering of the upper crust is a process of feldspar degradation accompanied by the formation of clay minerals. The loss of elements such as potassium, sodium, and calcium from feldspar minerals results in the accumulation of silica-alumina minerals in the products of weathering. To quantify the degree of weathering, the chemical index of alteration (CIA) was used. The CIA was calculated using the molecular proportions according to Equation (1):

$$CIA = Al_2O_3/(Al_2O_3 + CaO^* + Na_2O + K_2O) \times 100 \quad (1)$$

where CaO* represents the amount of CaO incorporated in the silicate fraction of the rock [56].

Because of the absence of a CO_2 value, the assumption proposed by Bock et al. was used [57]. After correcting for P_2O_5, if the mole fraction of CaO is less than that of Na_2O, the value of CaO is accepted. If, however, the mole fraction of CaO exceeds that of Na_2O, the mole fractions of CaO and Na_2O were assumed to be equal. In general, the CIA value of sandstone generated by weathering is ~70%, and it is unlikely to be lower than 50%. The average CIA value of the upper crust is ~47% [58], and a CIA value of 45–55% identifies unweathered sandstone. The CIA of the Jingxing Formation sample in the Munda section ranges from 59% to 78% (Table S1), with an average of 67%. The CIA of the Jingxing Formation sample of the Mangkang section ranged from 57% to 83%, with an average of

68%. The samples from both sections follow a trend of moderate chemical weathering. The CIA values of the Baishahe Formation (K_1p) in the Lanping-SiMao area range from 58% to 95%, with an average value of 82%. CIA values of mudstone samples from the Mengye jing (K_2me) Formation range from 45% to 55%, with an average of 74% [17,32]. The weathering intensity of the Simao area in Lanping is clearly lower than that in the Qamdo basin.

An A-CN-K triangle diagram is a further representation of the CIA value. This diagram can show the distribution of the analysis results of samples with different CIA values, and can be used to assess the composition of source rocks and the characteristics of the potassium metasomatism of samples [58,59]. The A-CN-K diagram (Figure 7) shows that both the Mangda and the Mangkang section reflect the same transition trend from low weathering to medium weathering, and the projected value is consistent with the calculated results. The weathering trend line slightly shifted to the right relative to the A-C-N edge, indicating that late weathering may have yielded in a small amount of elemental K.

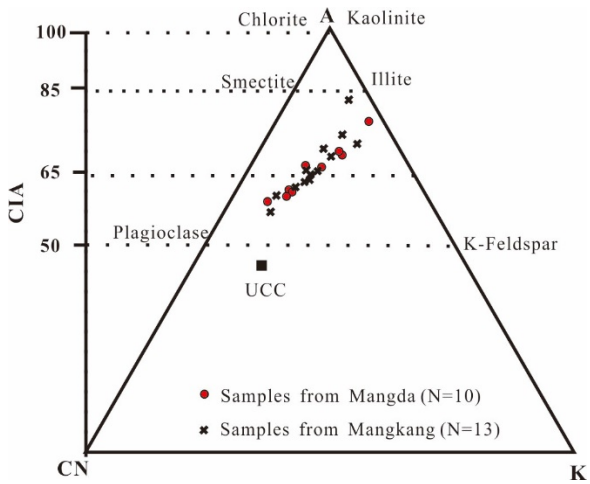

Figure 7. A-CN-K diagram of the sandstones in Qamdo district (after McLennan et al. [60] and Fedo et al.; [59]).

The detrital composition of sedimentary strata changes because of redeposition; therefore, it is necessary to distinguish samples for redeposition, i.e., by using the composition variation index, which is expressed in Equation (2):

$$ICV = [n(Fe_2O_3) + n(K_2O^*) + n(Na_2O) + n(CaO^*) + n(MgO) + n(MnO) + n(TiO_2)]/n(Al_2O_3) \quad (2)$$

where, n(CaO*) refers to n(CaO) in silicate, and $n(K_2O^*)$ represents the corrected $n(K_2O)$, i.e., the initial $n(K_2O)$ [59].

ICV > 1 indicates that the rock contains little clay minerals, which represents the first deposition in a tectonically active zone. ICV < 1 indicates that many clay minerals exist in the sediments, which may represent the first deposition under the conditions of re-deposition or enhanced weathering [60]. The ICV value of the Jingxing Formation sample in the Mangda section ranged from 0.6 to 1.2, with an average of 0.96 (Table S1). The ICV value of the Jingxing Formation in the Mangkang section ranged from 0.68 to 1.45, with an average of 1.2. This indicates that the Jingxing Formation in Qamdo Basin belongs to the first deposition type under the background of tectonic activity.

In the process of weathering, transporting, and sedimentation of rock, specific trace elements are not easily dissolved; therefore, they show the characteristics of parent rocks [61]. Cullers (1994) inferred that Cr/Th ratios of 2.5 to 17.5 are typical for felsic rocks [62]. The samples from the Jingxing Formation have Cr/Th ratios between 4.55 and 6.41, indicating a felsic source. The Th/Sc ratio is a good indicator of igneous chemical differentiation, and thus, a plot of Th/Sc versus Zr/Sc can reflect the degree of sedimentary sorting and recycling [58]. In Figure 8A, a portion of the analyzed samples evolved along the compositional variation

trend, but most samples belong to sediment recycling. More felsic rocks usually contain higher LREE/HREE ratios and negative Eu anomalies [63]. In this study, LREE/HREE ratios ranged between 7.23 and 11.01 and Eu/Eu* ratios ranged between 0.56 and 0.76, indicating a mostly felsic composition of the source area. This is consistent with the diagram of Eu/Eu* vs Th/Sc (Figure 8B). Successive cycles of weathering and redeposition can increase the Th/U ratios of sedimentary rocks and are thus good indicators of weathering and sedimentary recycling [58,64]. The Th/U ratios of samples range from 3.6 to 8.0, with ratios of most samples ranging between 3.6 and 6.3, slightly exceeding the average value of the UCC of 3.8 [65]. From the diagram of Th/U-Th, an increasing weathering trend can be observed, representing a moderate degree of weathering (Figure 8C).

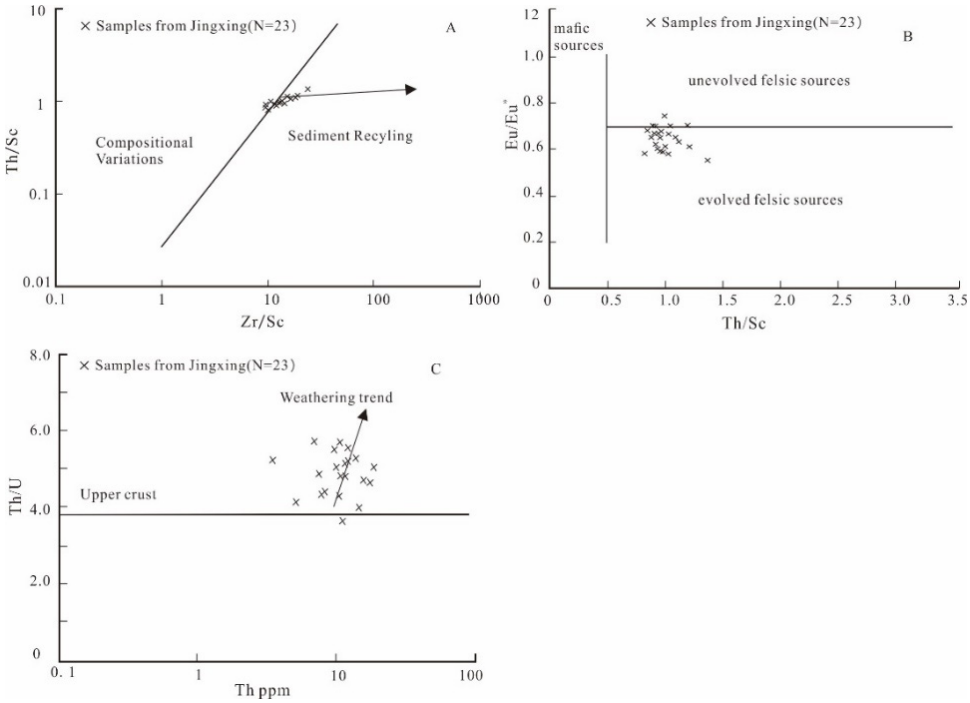

Figure 8. Discrimination diagrams illustrating sedimentary provenance. (**A**) Th/Sc versus Zr/Sc plot of samples (after McLennan et al., 1993 [58]). (**B**) Eu/Eu* versus Th/Sc of samples. (after McLennan et al., 1990 [66]). (**C**) Th/U versus Th, showing samples derived from felsic sources (after McLennan et al., 1993 [58]).

The sandstone of Jingxing Formation in Qamdo basin has sub-angular roundness and a high content of feldspar and lithic fragments. This indicates that the rock has a low compositional maturity and moderate weathering characteristics, reflecting the characteristics of strata close to the source area. The SiO_2/Al_2O_3 of the Jingxing Formation sandstones in Qamdo area ranges from 2.79 to 20.98, with an average of 7.91, indicating that the sandstone underwent moderate weathering [47]. The characteristics of Petrography, major elements, CIA values, and ICV together indicate that the weathering degree of the Early Cretaceous Jingxing Formation was low and characterized by near-source deposition. In this study, the trace elements of Jingxing Formation reflect a moderate degree of weathering and sediment recycling. By comparing the strata of the Jingxing Formation in the Qamdo basin with those of the Mengye jing Formation and the Baishahe Formation in the Lanping Simao basin shows that the weathering degree of the strata of Jingxing Formation in Qamdo area is lower than that of Lanping Simao area. The Early Cretaceous strata of the two basins have similar sediment recycling. It is possible that the sediments of the Early Cretaceous strata in this area are closer to the area of origin and have been deposited after a short transport.

5.2. Geochemical Provenance Signatures

Roser and Korsch studied the composition of sandstone protoliths based on whole-rock geochemistry. They established the discriminant function of the composition of F1-F2 sedimentary rocks based on the principal elements TiO_2, Al_2O_3, $Fe_2O_3{}^T$, MgO, CaO, Na_2O, and K_2O [67]. In this paper, four sedimentary stratigraphic types, including felsic igneus provenance, intermediate igneus provenance, quartzose sedimentary provenance, and magfic igneus provenance, are distinguished effectively. In Figure 9, most samples originate from the Jingxing Formation plot in the quartzose sedimentary provenance and felsic igneus provenance. This is basically consistent with the lithogeochemical classification diagram, indicating that the rocks of the Jingxing Formation originate from feldspar sandstone to lithic greywacke. This further indicates that the Jingxing Formation sandstone in Qamdo basin belongs to the category of quartz-rich sandstone.

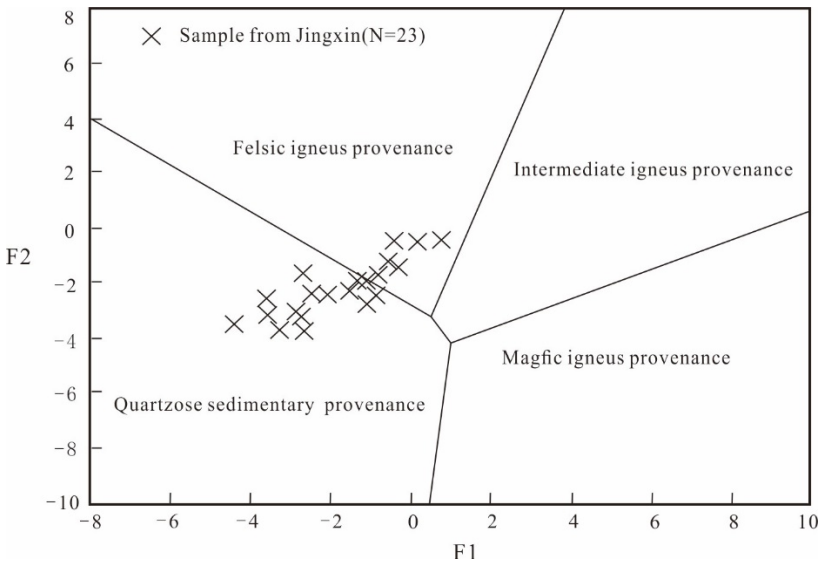

Figure 9. Major elemental composition discriminatory plots for the provenance of sandstones in Qamdo basin (F1 = $-1.773TiO_2 + 0.607Al_2O_3 + 0.76Fe_2OT_3 - 1.5MgO + 0.616CaO + 0.509Na_2O - 1.224K_2O - 9.09$; F2 = $0.445TiO_2 + 0.07Al_2O_3 - 0.25Fe_2OT_3 - 1.142MgO + 0.438CaO + 1.475Na_2O + 1.426K_2O - 6.861$, after Roser et al., 1988 [67]).

The chemical properties of alkaline earth metals (such as Sr and Ba) are similar, but the enrichment degree of these elements is slightly different in environments such as continental facies, alternating sea-land phase, and marine facies [68,69]. According to previous studies on the characteristics of sediments from the Pearl River Delta region of China, the contents of Sr and Ba in sediments of continental facies are less than 60 μg/g and 300 μg/g, while those in marine sediments exceed 160 μg/g and 400 μg/g, respectively. The differences between marine and continental facies sediments are large. The content of Sr in the sandstones of the Jingxing Formation from the Qamdo area ranges from 32.1 μg/g to 269 μg/g, with an average of about 122 μg/g, representing characteristics of marine and continental sedimentary facies. The Ba content of 127.0 μg/g to 421 μg/g, with an average of about 259.69 μg/g, shows the characteristics of continental sediments. Combined with the content distribution characteristics of Sr and Ba, the Jingxing Formation in the Qamdo area is characterized by typical marine-continental alternating sedimentary facies [70].

The geochemical characteristics of clastic sedimentary rocks are mainly determined by their composition, which is closely related to their origin and tectonic environment. The tectonic setting of diagenesis also partly controls the origin, and the chemical composition of sediment records the changes of tectonic activities over the process of sedimentation and diagenesis. Therefore, the composition of sedimentary rocks plays an important role in the tectonic setting of the area of origin. A specific relationship exists between the chemical

composition of sediments and the composition of clastic minerals, and their characteristics differ in response to different tectonic environments. Therefore, the properties and tectonic background of the area of origin can be determined according to the composition variation characteristics. Based on data of sandstone and arenaceous rocks, a series of geochemical endmember maps of major elements are proposed to identify the tectonic setting of the passive continental margin, the active continental margin, the oceanic island arc, and the continental island arc. Mutual correction among these different endmember maps has been adopted by most scholars [26]. The present study adopted the diagram of SiO_2-K_2O/Na_2O [71] and (SiO_2 / 20)—(K_2O + Na_2O)—(TiO_2 + FeO + MgO) [72] to conduct drop point analysis on all sandstone samples in the study area, as shown in Figure 10. Both Cretaceous Jingxing Formation samples fall into the range of active continental margin and passive continental margin.

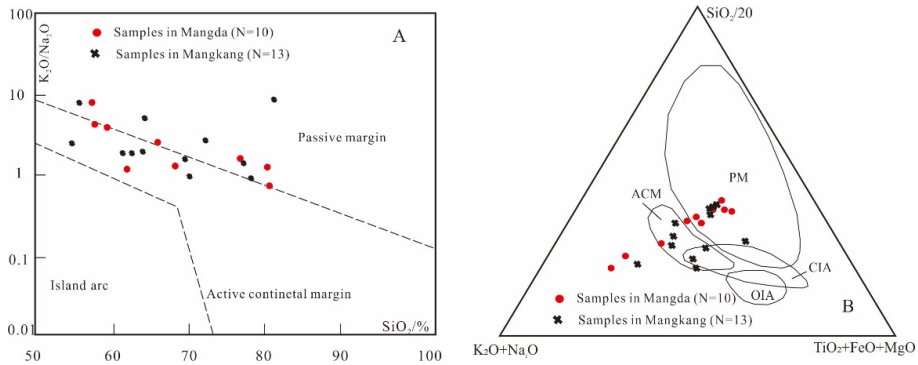

Figure 10. Tectonic setting discrimination diagrams based on the major elements for Jingxing Formation sandstones of Qamdo district (**A** after Bhatia and Crook [71], and **B** after Kroonenberg [72]). Abbreviations: OIA, ocean island arc; CIA, continental island arc; ACM, active continental margin; PM, passive margin.

The basic assumption of the geochemical discrimination of sedimentary rocks is that a close relationship exists between the plate tectonic environment and the origin of sedimentary rocks. However, one of the major uncertainties is that particular sediments may migrate from the tectonic setting of their origin to the sedimentary basin of a different tectonic setting. In contrast to major element analysis, the contents of stable trace elements and REE are mainly controlled by the rock composition of their origin, reflecting the elemental spherochemistry of their area of origin [73]. According to the discriminant diagram of the trace element tectonic background as proposed by Bhatia et al. (1986) [27], clastic rock deposits in the study area were analyzed.

Figure 11 shows that the stratigraphic tectonic setting of the Cretaceous Jingxing Formation in Qamdo basin is a relatively stable active continental margin and passive continental margin, with characteristics of a continental island arc. The Cr/Ni ratio ranges from 1.0 to 2.5, indicating a very low content of mafic or ultramafic rocks in the source region [74]. At the crustal scale, most trace elements of Zr occur in zircon grains, and most HREE and trace elements are affected by zircon grains. The Zr/Hf ratios of zircon grains range from 30 to 40 [75], and the Zr/Hf value of the JingXing Formation sandstones ranges from 30.17 to 34.73. These results indicate that the Zr and Hf contents are controlled by detrital zircon grains. The Nb/Ta ratio of the upper crust is about 12 [76], and the Nb/Ta ratio of the Jingxing Formation sandstone ranges from 10.28 to 12.03, with an average of 11.07. These geochemical characteristics indicate that both Nb and Ta elements in the sandstone may mainly originate from upper crustal rock units. The Sr/Ba ratio reflects the palaeosalinity characteristics of the sedimentary environment. It is generally assumed that the Sr/Ba ratio of marine sediments with high salinity exceeds 1.0, while the Sr/Ba ratio of freshwater sediments is generally lower than 1.0 [70]. The Sr/Ba ratio of sandstone samples from the Jingxing Formation is less than 1.0, except for MK15 (1.79), which indicates that

the sedimentary environment of Jingxing Formation is continental. Regional lithofacies paleogeographic studies also showed that the Tethys Ocean on the western side of Qamdo basin gradually closed from the Middle and Late Jurassic to the end of the Early Cretaceous. Afterwards, the Qamdo area, as a marginal sea of the continental margin, ended marine sedimentation and formed continental lacustrine basin deposits [77]. During the evolution of the Tethys Ocean, Qamdo belonged to a landmass in a multi-island arc system [52]. Previous studies showed that the samples of Pashahe Formation and Mangang Formation of Early Cretaceous strata in the Lanping-Simao area, as well as the provenance of Mengye jing Formation of Late Cretaceous strata, mainly originate from passive continental margin environment. A small amount originates from an active continental margin environment. Few samples showed that the origin in this area had the nature of a continental island arc [17,32], which was basically similar to the results of the present study. This indicates that the tectonic background of the Cretaceous strata in Qamdo area and Lanping Simao Cretaceous strata were basically identical.

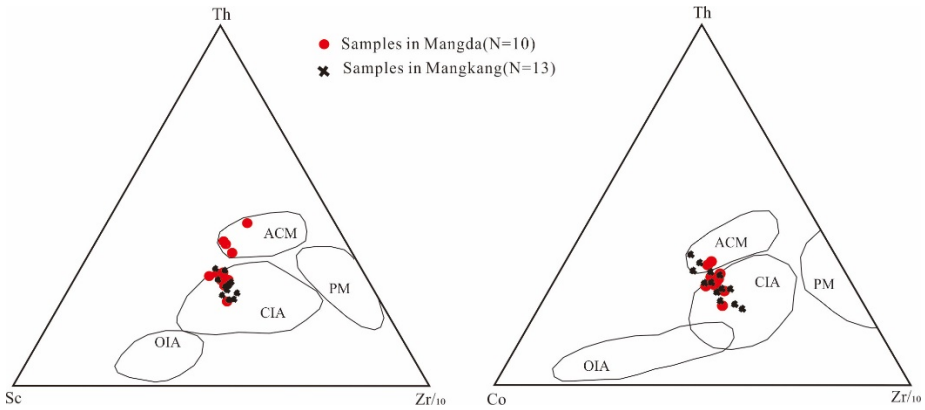

Figure 11. Tectonic setting discrimination diagrams based on the trace elements of Jingxing Formation sandstones from the Qamdo district. Abbreviations: OIA, ocean island arc; CIA, continental island arc; ACM, active continental margin; PM, passive margin (after Bhatia et al.; 1986 [27]).

5.3. Detrital Zircon Provenance

The LA-ICP-MS concordant ages of detrital zircon grains from the Jingxing Formation sandstone samples in Qamdo area mainly range from 198 Ma to 608 Ma, 721 Ma to 1006 Ma, and 1694 Ma to 2082 Ma. The zircon ages mainly show two peaks at 450 Ma and 1870 Ma. In Lanping-Simao basin, the youngest cluster of ages in Mengye jing Formation ranges from 215 Ma to 218 Ma, shows a peak of Late Ordovician ages (at 449 Ma), with ages ranging from 414 Ma to 472 Ma [17], and is similar to the peak age of 450 Ma in Qamdo basin. The latest age of detrital zircon grains in sedimentary rocks indicates the lower limit of their formation [78]. The minimum age of detrital zircon grains in the Jingxing formation in the Qamdo area is 195.4 Ma, which represents the lower limit of its deposition. The deposition of the Jingxing Formation in the Qamdo area should be later than the early Jurassic. According to the study of detrital zircon grains in the Mengye jing Formation, the provenance of the detrital zircon grains is mainly Qiangtang block, Ailaoshan tectonic belt, and Yangtze plate. In this study, the age range of 198–608 Ma is very consistent with the age distribution characteristics of the southern Qiangtang Block, Songpan-Ganzi Block, Ailaoshan Tectonic Belt, Youjiang basin, and Lanping Simao basin. The age range from 721 Ma to 1006 Ma is consistent with the origin ages of the Southern Qiangtang Block, the Yangtze Block, and the Lanping Simao basin. The age range of 1694–2082 Ma is consistent with the age distribution characteristics of the Southern Qiangtang Block, Songpan-Ganzi Block, and Lanping Simao basin (Figure 12). Based on the age distribution characteristics of the three groups, the main detrital origin of the Jingxing Formation in the Qamdo area is concentrated in the Early Cambrian to Early Jurassic, and shares the age characteristics of the Neoproterozoic. The age distribution shows that the provenance area of the Jingxing

Formation is mainly north Qiangtang Block, Qiangtang Block, Songpan-Ganzi Block, and Youjiang basin. The clastic ages of the Qamdo-Lanpingsimao basin are highly consistent, indicating that the Cretaceous strata of the two basins have the same provenance.

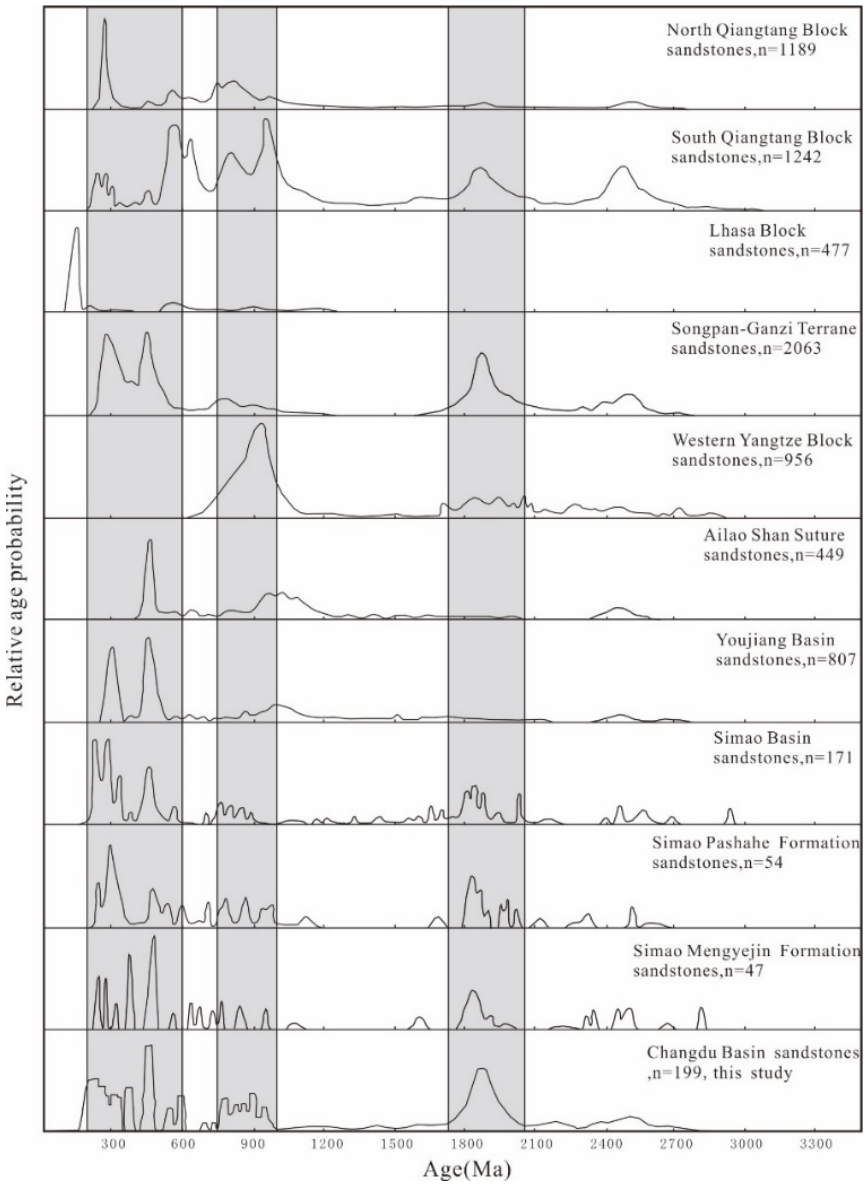

Figure 12. Probability density plots and histograms of LA-ICP-MS detrital zircon U-Pb ages of the Qamdo samples compared with those from Qiangtang (after Gehrels et al., 2011 [79]), Lhasa (after Leier et al., 2007 [80]), Songpan-Ganzi (after Weislogel et al., 2010 [81]), Yangtze (after Zhao et al., 2010 [82]), Ailaoshan (after Lai, 2012 [83]), Youjiang basin (after Yang et al., 2012 [84]), Simao basin (after Wang et al., 2014 [17]), and Pashahe and Myejing Formations (after Li et al., 2015 [18]).

Previous studies showed that the basement of the Himalayan Block and Lhasa Block south of the Bangonglake-Nujiang Suture Zone is a pan-African basement. Pan-African tectono-magmatic heat events of the pre-Ordovician metamorphic basement are widely developed [85,86]. In recent years, Pan-African age records have been successively found in the metamorphic basement of the northern Qiangtang Block. The Pan-African orogeny occurred between 600 Ma and 500 Ma, and the age obtained from the Jitang metamorphic complex (520–570 Ma) is similar to that of the Pan-African orogeny [87,88]. The peak age of 450 Ma is close to that of the end of the Pan-African movement, indicating that the

sediments of the Jingxing Formation in the Qamdo area may have originated from an orogenic source area that experienced Pan-African movement.

The basement of the Qamdo basin consists of Jitang metamorphic rocks. Its formation age is generally considered to be ancient (i.e., either Mesoproterozoic or Precambrian). The composition and geochemical characteristics of the original rocks identified them as island arc volcanic rocks and pyroclastic rocks of 1700–1900 Ma, which are the volcanic products of the active continental margin west of the Yangtze continent. The Ningduo Group is distributed in the eastern part of the Qamdo-Simao Block and consists of a set of metamorphic gneiss, granulite, schist, and marble with medium depth. In the Ningduo black cloud plagenous gneiss U-Pb age curve, the upper intersection point is 1870 ± 280 Ma, and the lower intersection point is 490 ± 130 Ma. Sm-Nd isochron ages of 1593.975 ± 240.5 Ma have been obtained from the plagioclase gneiss of pomegranate musca [89]. In the present study, the peak age of this detrital zircon at 1870 Ma suggests that the metamorphic rock series of Jitang Group and Ningduo Group in the basement of the Qamdo Block provide abundant origin for the strata of the Jingxing Formation in the Qamdo Basin.

6. Implications for Late Cretaceous Potassium Mode in the Eastern Tethys

The East Tethys lithofacies paleogeography shows that in the Late Triassic, the Nujiang Tethys oceanic crust subducted under the southern Qiangtang-Zuogong Block. The collision of the Dege Block with the Qamdo Block resulted in the uplift of the western margin of the southern Qiangtang-Zuogong Block and the eastern margin of the Qamdo-Simao Block, leading to the formation of the Qamdo-Mangkang basin. At this time, the basin developed fluvial-lacustrine facies, coastal facies, shallow marine facies, and sea–land intersedimentation [16]. In the Middle Jurassic, the Nujiang Tethys Ocean gradually closed from east to west. Furthermore, the Qamdo-Lanping-Simao land block closed and became a unified and large basin, with local residual sea areas of the Neo-Tethys Ocean and intercontinental marine deposits with continental crust as seafloor [16]. In the late Cretaceous period, the Qamdo-Simao-Khorat land distribution is nearly east–west oriented (paleomagnetic), and Qiangtang basin and Qamdo area are widely distributed shallow sea and coastal depositions [90]. Jurassic and Cretaceous gypsum deposits in Qamdo basin and magnesite deposits in the Middle Jurassic Yanshiping are typical representatives of this formation. According to the field geological characteristics, magnesite has typical sedimentary genetic characteristics in Baxia, Qamdo basin.

When normal seawater evaporates to the end of the salt stage, magnesite can be precipitated when the Mg/Ca ratio reaches suitable conditions and with the doping of terrestrial water containing Ca and HCO^{3-} [18]. Analysis of the experimental model showed that the eastern Qiangtang area generally lacks salt mineral deposits, while the Lanping Simao area lacks the corresponding sulfate and magnesium-bearing carbonate (magnesite) precipitations, while it contains many potassium salt deposits. The sulfur isotopic composition of gypsum of the Yunlong Formation in the Lanping basin also indicates that it is of marine origin [19]. The Br geochemistry of potash evaporite rocks of the Mengye jing Formation in the Simao basin and the sulfur isotopic characteristics of anhydrite also indicates marine origin [18]. The sulfur and strontium isotopic values of gypsum in the Qamdo Basin also point toward marine origin [18]. In this study, the age distribution of detrital zircon grains in the Jingxing Formation indicates that the Qiangtang Block, the Ailaoshan Tectonic Belt, and the Yangtze area constitute the origin of the Qamdo-Lanping-Simao basin. The minimum age of detrital zircon grains from the Jingxing Formation in the Qamdo Basin is 195.4 Ma, and the minimum age of detrital zircon grains from the Baishahe Formation (K_1P) in the Lanping-Simao basin is 210 Ma [18]. The above-mentioned studies further suggest that the two basins began to receive unified deposits after the Early Jurassic at the latest [78]. In this paper, petrographic and geochemical studies showed that Qamdo Basin is closer to the source area than the Lanping Simao basin. In the Late Cretaceous, the Qamdo basin was deposited in the Lanping Simao basin with a large number of potash deposits, which had a distinct characteristic of a preparatory basin.

In conclusion, the Qamdo-Lanping Simao basin has a similar and unified tectonic evolution background with regard to its regional evolution history. In terms of geochemical characteristics of sedimentary strata and origin characteristics of detrital zircon grains, many similarities exist between both sources. The Early Cretaceous strata of the Qamdo-Lanping-Simao basin began to receive a unified origin deposit at the latest after the Middle Jurassic. Both basins may have been marine submersion basins with a unified hydraulic connection before evaporite deposition. Nujiang Tethys ended its evolution in the Late Cretaceous, and the Nujiang area continued its collision orogeny; therefore, the metamorphic seawater remaining in Qamdo basin may have migrated from Qamdo basin to Lanping-Simao basin and even to Khorat basin under the influence of orogeny. Thus, large amounts of evaporite and potassium salts were deposited in these areas (Figure 13).

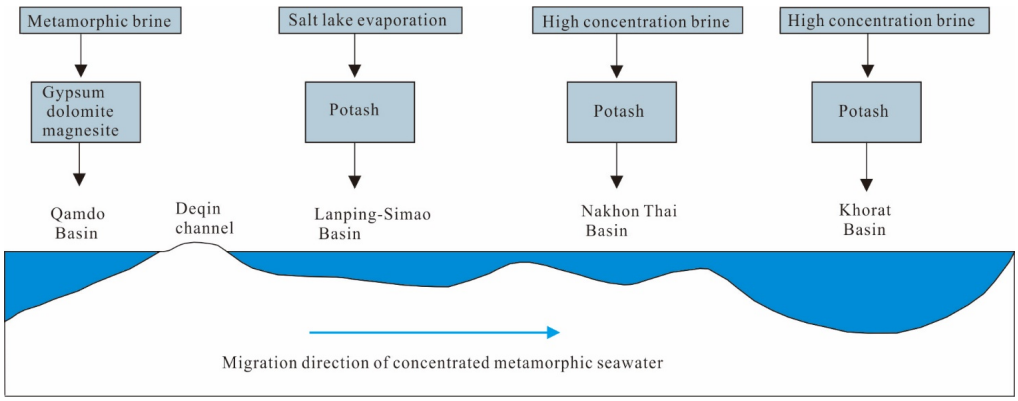

Figure 13. Metallogenic model of Cretaceous evaporation deposit in Lanping-Simao-Korat basin (modified after Li, 2015 [18]).

7. Conclusions

The petrography shows that the weathering degree of the sandstone in Jingxing Formation is low. The geochemistry of sandstones also indicates moderate weathering conditions and a predominantly felsic source with minor recycled sediments. In combination, the main trace whole rock geochemistry and weathering indexes indicate that the Early Cretaceous Jingxing Formation in the Qamdo basin have a lower weathering degree than those in the Lanping Simao district; moreover, the Qamdo basin is closer to the source erosion area.

The stratigraphic tectonic setting of the Early Cretaceous Jingxing Formation in the Qamdo basin is mainly composed of a relatively stable active continental margin and a passive continental margin, with continental island arc characteristics. Trace element data indicate that the sedimentary environment of the Jingxing Formation is continental. The Early Cretaceous Jingxing Formation in the Qamdo district and the Cretaceous strata in the Lanping Simao district share the same tectonic setting.

The main age peaks of detrital zircon grains from the Jingxing Formation in the Qamdo area are 198–608 Ma, 721–1006 Ma, and 1694–2082 Ma. The minimum age is 195.4 Ma, which represents the lower limit of the deposition, and the deposition of the Jingxing formation most likely happened after the Early Jurassic. The age distribution characteristics of detrital zircon grains indicate that the origin of the Early Cretaceous strata in both Qamdo and Lanping Simao basin is related, and the main areas of origin are Qiangtang Block, Songpan-Ganzi Block, and Youjiang basin. Combined with the regional evolutionary background and analysis of the detrital zircon age, the Early Cretaceous strata in the Qamdo-Lanping-Simao basin began to receive the same deposits at the latest after the Early Jurassic. Both basins may have been marine submersion basins with the same water resource connection before evaporite deposition. Under the influence of tectonic movement, the residual metamorphic seawater in Qamdo basin may have migrated from Qamdo basin

to Lanping-Simao basin and even to Khorat basin, where it may have deposited a large volume of evaporite and potassium salt.

Supplementary Materials: The following are available online at https://www.mdpi.com/article/10.3390/min11070745/s1, Table S1: Whole-rock geochemical compositions of Jingxing Formation sandstones from Qamdo, Table S2. LA-ICP-MS zircon U-Pb age data results of sandstones from Jingxing Formation in Qamdo Basin. References [91,92] are cited in Supplementary Materials.

Author Contributions: Conceptualization, W.H. and H.M.; methodology, W.H.; software, W.H.; validation, H.M and H.C.; formal analysis, W.H.; investigation, W.H., H.M., H.C., B.L., Y.L., W.M., and Q.H; resources, H.M.; data curation, H.M.; writing—original draft preparation, W.H.; writing—review and editing, H.M., W.F., H.C., B.L., Y.L., W.M., and Q.H.; visualization, W.H. and H.M.; supervision, H.M.; project administration, H.M.; funding acquisition, H.M. All authors have read and agreed to the published version of the manuscript.

Funding: This work was funded by the National Key Basic Research Project of China (973 program, No. 2011CB403004).

Data Availability Statement: Not applicable.

Acknowledgments: We are very grateful to the lab staff of the Beijing Research Institute of Uranium Geology, Beijing, China, and the State Key Laboratory of Continental Dynamics, Northwest University, Xian, China. Valuable comments and suggestions of three anonymous reviewers are acknowledged.

Conflicts of Interest: The authors declare no conflict of interest.

References

1. Pan, G.T.; Wang, L.Q.; Li, R.S. Tectonic model of archipelagic arc-basin systems: The key to the continental geology. *Sediment. Geol. Tethyan Geol.* **2012**, *32*, 1–20.
2. Wu, F.Y.; Wan, B.; Zhao, L.; Xiao, W.J.; Zhu, R.X. Tethyan geodynamics. *Acta Petrol. Sin.* **2020**, *36*, 1627–1674.
3. Wang, J.; Tan, F.W.; Wang, X.L.; Du, M.W.; Chen, M. The Sedimentary and Tectonic Characteristics of Qiangtang Basin in the Early Jurassic in Northern Xizang (Tibet). *Acta Sedimentol. Sin.* **2004**, *22*, 198–205.
4. Wang, J.; Fu, X.G.; Li, Z.X.; Xiong, S. Formation and significance of the shales from North Qiangtang basin. *Sediment. Geol. Tethyan Geol.* **2010**, *30*, 11–17.
5. Wang, J.; Fu, X.G.; Tan, F.W.; Chen, M.; He, J.L. A new sedimentary model for Qiangtang basin. *Acta Sedimentol. Sin.* **2010**, *5*, 884–893.
6. Xia, G.Q.; Yi, H.S.; Huang, H.G.; Wu, X.F.; Hui, B. Meter-scale sedimentary cycles and genesis of Xiali Formation in Yanshiping area, Northern Tibet. *J. Chengdu Univ. Technol.* **2010**, *37*, 133–139.
7. Su, T.N.; Zhang, W.Z.; Zhang, S.Z.; Zhang, H. Geologic features of gypsum strata in the middle part of Buqu Formation, Biluocuo area, Tibet. *Jilin Geol.* **2007**, *26*, 10–15.
8. Li, Y.L.; Wang, C.S.; Li, T.N. Characteristics of the Jurassic saline deposits and its significance to hydrocarbon accumulation in Qiangtang basin of Tibet area. *Acta Pet. Sin.* **2008**, *29*, 17–178.
9. Li, Z.X.; He, J.L.; Xiong, X.G.; Wu, T.; Bai, P.R. The upper Jurassic-Lower Cretaceous shenglihe oil shales and their formation in the Qiangtang basin, northern Xizang. *J. Jilin Univ. Earth Sci. Ed.* **2010**, *40*, 264–272.
10. Wu, T.; Xiong, X.G.; Yi, C.X.; Bai, P.R.; He, Y.Z.; Liu, Z.C. Gypsolyte sedimentary environment of upper Jurassic-Lower Cretaceous in shenglihe area in northern Qiangtang basin. *Xinjiang Pet. Geol.* **2010**, *31*, 376–378.
11. Zheng, M.P.; Yuan, H.R.; Zhang, Y.S.; Liu, X.F.; Chen, W.X.; Liu, J.S. Regional Distribution and Prospects of Potash in China. *Acta Geol. Sin.* **2010**, *84*, 1526–1553.
12. Niu, X.S.; Chen, W.X.; Liu, X.F. Geochemial characteristics on salt springs and potash perspective in dogai coring area of Qiangtang basin. *Geoscience* **2013**, 621–628.
13. Qu, Y.H. Homology of potassium-bearing brine from Lanping-Simao basin and Khorat basin, Thailand. *Geol. Chem. Miner.* **1997**, *19*, 81–84.
14. Yuan, Q.; Qin, Z.J.; Wei, H.C.; Sheng, S.R.; Shan, F.S. The Ore-forming Age and Palaeoenvironment of the Mengyejing Formation in Jiangcheng, Yunnan Province. *Acta Geosci. Sin.* **2013**, *5*, 631–635.
15. Wang, L.C.; Liu, C.L.; Fei, M.M.; Shen, L.J.; Zhang, H.; Zhao, Y.J. First SHRIMP U-Pb zircon ages of the potash-bearing Mengyejing Formation, Simao Basin, southwestern Yunnan, China. *Cretac. Res.* **2015**, *52*, 238–250. [CrossRef]
16. Xie, X.W. *Report of Regional Geological Survey: Nangqian County, Qamdo County, Jiangda County*; Tibet Institute of Geological Survey: Tibet, China, 2007; pp. 107–109.

17. Wang, L.C.; Liu, C.L.; Gao, X.; Zhang, H. Provenance and paleogeography of the Late Cretaceous Mengyejing Formation, Simao Basin, southeastern Tibetan Plateau: Whole-rock geochemistry, U–Pb geochronology, and Hf isotopic constraints. *Sediment. Geol.* **2014**, *304*, 44–58. [CrossRef]
18. Li, Y.S. Metallogenic Model of the Cretaceous Potassium-Bearing Evaporites Involving Changdu, Lanping-Simao and Khorat Basin. Ph.D. Thesis, University of Chinese Academy of Sciences, Beijing, China, 2015.
19. Wang, L.C.; Liu, C.L.; Fei, M.X.; Shen, L.J.; Zhang, H. Sulfur isotopic composition of sulfate and its geological significance of the Yunlong formation in the Lanping basin, Yunnan Province. *China Min. Mag.* **2014**, *23*, 57–63.
20. Gao, X.; Fang, Q.F.; Yao, W.; Peng, Q.; Dong, J.; Qin, H.; Di, Y.W. Genesis of the Mengyejing potash deposit in Lanping-Simao basin, Yunnan: Indication from the components of the ceposit. *Acta Geosci. Sin.* **2013**, *34*, 529–536.
21. Hite, R.J.; Japakasetr, T. Potash deposits of the Khorat Plateau, Thailand and Laos. *Econ. Geol.* **1979**, *74*, 448–458. [CrossRef]
22. Fedo, C.M.; Sircombe, K.N.; Rainbird, R.G. Detrital zircon analysis of the sedimentary record. *Rev. Mineral. Geochem.* **2003**, *53*, 277–303. [CrossRef]
23. Gehrels, G. *Detrital Zircon U–Pb Geochronology: Current Methods and New Opportunities*; Wiley-Blackwell: Busby, Australia, 2012; pp. 47–62.
24. Wu, F.Y.; Yang, J.H.; Wilde, S.A.; Liu, X.M.; Guo, J.H.; Zhai, M.G. Detrital zircon U–Pb and Hf isotopic constraints on the crustal evolution of North Korea. *Precambrian Res.* **2007**, *159*, 155–177. [CrossRef]
25. Shen, C.B.; Mei, L.F.; Peng, L.; Chen, Y.Z.; Yang, Z.; Hong, G.F. LA-ICPMS U–Pb zircon age constraints on the provenance of Cretaceous sediments in the Yichang area of the Jianghan Basin, central China. *Cretac. Res.* **2012**, *34*, 172–183. [CrossRef]
26. Bhatia, M.R. Plate tectonics and geochemical composition of sandstones. *J. Geol.* **1983**, *91*, 611–627. [CrossRef]
27. Bhatia, M.R.; Crook, K.W. Trace element characteristics of graywackes and tectonic setting discrimination of sedimentary basins. *Contrib. Mineral. Petrol.* **1986**, *92*, 181–193. [CrossRef]
28. Song, Y.C.; Hou, Z.Q.; Yang, T.N.; Zhang, H.R.; Yang, Z.S.; Tian, S.H.; Liu, Y.C.; Wang, X.H.; Liu, Y.X.; Xue, C.D.; et al. Sediment-Hosted Himalayan Base Metal Deposits in Sanjiang Region: Characteristics and Genetic Types. *Acta Petrol. Mineral.* **2011**, *30*, 355–380.
29. Qin, X.W.; Ma, H.Z.; Zhang, X.Y.; Fan, Q.S.; Cheng, H.D.; Li, Y.S.; Miao, W.L.; Hai, Q.Y.; Shi, H.Y. Hydrochemical Characteristics of Salt Spring and Potassium-Prospecting in Changdu Ba-sin. *J. Salt Lake Res.* **2017**, *25*, 28–39.
30. Wang, L.C.; Liu, C.L.; Shen, L.J.; Bo, Y. Research Advances in Potash Forming of the Simao Basin, Eastern Tethyan Realm. *Acta Geol. Sin.* **2018**, *92*, 1707–1723.
31. Hou, Z.Q.; Lu, J.R.; Li, H.Y.; Wang, D.H.; Lu, Q.T. Tectonic evolution of the Tethys in southwestern China: Is controlled by plume tectonics. *Acta Geosci. Sin.* **1996**, *17*, 439–451.
32. Miao, W.L. Sedimentary Characteristics and Source Links between Lanping-Simao and Khorat Basins, Based on the Analysis of Clastic Rocks of Salt-Bearing/Underlying Stratas; Implication for Regional Salt-Forming Setting. Ph.D. Thesis, University of Chinese Academy of Sciences, Beijing, China, 2016.
33. Peng, Y.M.; Liu, J.Y. Triassic lithofacies and palaeogeography in Qamdo, east Tibet. *J. Palaeogeoography* **1994**, *4*, 26–34.
34. Ye, H.F.; Luo, J.N.; Li, Y.T.; Tong, Z.Y.; Yu, Q.; Wang, X.L.; Zhu, T.X.; Feng, X.T. Tethyan tectonic domain and petroleum exploration. *Sediment. Geol. Tethyan Geol.* **2000**, *01*, 1–27.
35. Luo, J.N.; Wang, X.L.; Li, Y.T.; Zhu, Z.F.; Feng, X.T.; Xie, Y. Sedimentary geological evolution of the Qinghai-Xizang Tethys. *Sediment. Geol. Tethyan Geol.* **2002**, *1*, 7–15.
36. Yan, T.; Wu, G.Y.; Tang, M.Q. Tectono-sedimentary development of backarc continental basin in Yunnan, southern China. *J. Southeast Asian Earth Sci.* **1994**, *9*, 153–166. [CrossRef]
37. He, L.Q. Tectonic seting and evolutionary pattern of Jinshajiang orogenic belt. *Geoscience* **1998**, *12*, 185–191.
38. Ding, L.; Kapp, P.; Yue, Y.H. Postcollisional calc-alkaline lavas and xenoliths from the southern Qiangtang terrane, central Tibet. *Earth Planet. Sci. Lett.* **2007**, *254*, 28–38. [CrossRef]
39. Zhang, K.J. Blueschist-bearing metamorphic core complexes in the Qiangtang block reveal deep crustal structure of northern Tibet: Comment and Reply. *Geology* **2001**, *29*, 91–95. [CrossRef]
40. Tan, F.W.; Wang, G.M.; Hui, L. The relationship betwwen cenozioc tectonic regime and mineralization in eastern Tibet. *Acta Geosci. Sin.* **2001**, *22*, 123–128.
41. Wang, Z.Z.; Tan, F.W.; Chen, M. Sedimentary-tectonic evolution and hydrocarbon potential in the Qamdo basin, eastern Xizang. *Sediment. Geol. Tethyan Geol.* **2018**, *38*, 85–96.
42. Chen, H.H.; Wu, Y.; Xiao, Q.G.; He, S. Fluid Inclusion Evidence of Paleo-Oil Reservoirs in Changdu Basin, Tibet. *Act Geol. Sin.* **2010**, *84*, 1457–1469.
43. Cullen, J.T.; Field, M.P.; Sherrell, R.M. Determination of trace elements in filtered suspended marine particulate material by sector field HR-ICP-MS. *J. Anal. At. Spectrom.* **2000**, *16*, 1307–1312. [CrossRef]
44. Ludwig, K.R. *User's Manual for Isoplot 3.23: A Geochronological Toolkit for Microsoft Excel*; Special Publication; Berkeley Geochronology Center: Berkeley, CA, USA, 2003; pp. 1–71.
45. Hou, K.J.; Li, Y.H.; Tian, Y.R. In situ U–Pb zircon dating using laser ablation-multiion counting-ICP-MS. *Miner. Depos.* **2009**, *28*, 481–492.
46. Taylor, S.R.; McClennan, S.R. *The Continental Crust: Its Composition and Evolution*; Blackwell Scientific Publication: Oxford, UK, 1985; pp. 1–312.

47. Pettijohn, F.J.; Potter, P.E.; Siever, R. *Sand and Sandstone*; Springer: New York, NY, USA, 1972; pp. 148–290.
48. Asiedu, D.K.; Suzuki, S.; Nogami, K.; Shibata, T. Geochemistry of Lower Cretaceous sediments, Inner Zone of Southwest Japan: Constraints on provenance and tectonic environment. *Geochem. J.* **2000**, *34*, 155–173. [CrossRef]
49. Pullen, A.; Kapp, P.; Gehrels, G.E.; Vervoort, J.D.; Ding, L. Triassic continental subduc-tion in central Tibet and Mediterranean-style closure of the Paleo-Tethys Ocean. *Geology* **2008**, *36*, 351–354. [CrossRef]
50. Wu, Y.B.; Zheng, Y.F. Genesis of zircon and its constraints on interpretation of U-Pb age. *Chin. Sci. Bull.* **2004**, *49*, 1554–1569. [CrossRef]
51. Belousova, E.A.; Griffin, W.L.; O'Reilly, S.Y.; Fisher, N.I. Igneous zircon: Trace element composition as an indicator of source rock type. *Contrib. Mineral. Petrol.* **2002**, *143*, 602–622. [CrossRef]
52. Hoskin, P.W. Rare earth element chemistry of zircon and its use as a provenance indicator. *Geology* **2001**, *28*, 627–630. [CrossRef]
53. Vavra, G.; Schmid, R.; Gebauer, D. Internal morphology, habit and U-Th-Pb microanalysis of amphibolite-to-granulite facies zircons grains: Geochronology of the Ivrea Zone (Southern Alps). *Contrib. Mineral. Petrol.* **1999**, *134*, 380–404. [CrossRef]
54. Johnson, M.J. *The System Controlling the Composition of Clastic Sediments*; Geological Society of America: Boulder, CO, USA, 1993; pp. 1–19.
55. Wedepohl, K.H. Composition and abundance of common igneous rocks. In *Handbook of Geochemistry*; Wedepohl, K.H., Ed.; Springer: Berlin/Heidelberg, Germany, 1969; pp. 272–279.
56. Nesbitt, H.W.; Young, G.M. Early proterozoic climates and plate motions inferred from major element chemistry of lutites. *Nature* **1982**, *299*, 715–717. [CrossRef]
57. Bock, B.; McLennan, S.M.; Hanson, G.N. Geochemistry and provenance of the middle Ordovician Austin Glen member (Normanskill formation) and the Taconian orogeny in New England. *Sedimentology* **1998**, *45*, 635–655. [CrossRef]
58. McLennan, S.M.; Hemming, S.; McDaniel, D.K.; Hanson, G.N. Geochemical approaches to sedimentation, provenance, and tectonics. *Geol. Soc. Am.* **1993**, *284*, 21–40.
59. Fedo, C.M.; Nesbitt, H.W.; Young, G.M. Unraveling the effects of potassium metasomatism in sedimentary rocks and paleosols, with implications for paleoweathering conditions and provenance. *Geology* **1995**, *23*, 921–924. [CrossRef]
60. Culllers, R.L.; Podkovyrov, V.N. The source and origin of ter-rigenous sedimentary rocks in the Mesoproterozoic Ui group, southeastern Russia. *Precambrian Res.* **2002**, *117*, 157–183. [CrossRef]
61. Jorge, R.C.; Fernandes, P.; Rodrigures, B.; Pereira, Z.; Oliveira, J.T. Geochemistry and provenance of the Carboniferous Baixo Alentejo Flysch Group, South Portuguese Zone. *Sediment. Geol.* **2013**, *284–285*, 133–285. [CrossRef]
62. Cullers, R.L. The controls on the major and trace element variation of shale, siltstone and sandstone of Pennsylvanian-Permian age from uplifted continental blocks in Colorado to platform sediment in Kansas, USA. *Geochim. Cosmochica Acta* **1994**, *58*, 4955–4972. [CrossRef]
63. Cullers, R.L. The controls on the major-element and trace-element evolution of shales, siltstones and sandstones of Ordovician to Tertiary age in the Wet Mountains Region, Colorado, USA. *Chem. Geol.* **1995**, *123*, 107–131. [CrossRef]
64. McLennan, S.M.; Taylor, S.R. Th and U in sedimentary rocks: Crustal evolution and sedimentary recycling. *Nature* **1980**, *285*, 621–624. [CrossRef]
65. McLennan, S.M.; Taylor, S.R.; Hemming, S.R. *Composition, Differentiation, and Evolution of Continental Crust: Constrains from Sedimentary Rocks and Heat Flow*; Cambridge University Press: Cambridge, UK, 2006; pp. 92–134.
66. McLennan, S.M.; Taylor, S.R.; McCulloch, M.T.; Maynard, J.B. Geochemical and Nd–Srisotopic composition of deep-sea turbidites-crustal evolution and plate tectonic associations. *Geochim. Cosmochim. Acta* **1990**, *54*, 2015–2050. [CrossRef]
67. Roser, B.P.; Korsch, R.J. Provenance signatures of sandstone- mudstone suites determined using discriminant function analysis of major-element data. *Chem. Geol.* **1988**, *67*, 119–139. [CrossRef]
68. Deng, P. The application of trace amount of elements in the exploration of oil and gas. *Pet. Explor. Dev.* **1993**, *20*, 27–35.
69. Liu, G.; Zhou, D.S. Application of microelements analysis in identifying sedimentary environment. *Pet. Geol. Exp.* **2007**, *29*, 307–310.
70. Lan, X.H.; Ma, D.X.; Xu, M.G.; Zhou, Q.W.; Zhang, G.W. Geochemical markers and facies significance in the Pearl River Delta. *Mar. Geol. Quat. Geol.* **1987**, *7*, 39–49.
71. Roser, B.P.; Korsch, R.J. Determination of tectonic setting of sandstone-mudstone suites using SiO_2 content and K_2O/Na_2O ratio. *J. Geol.* **1986**, *94*, 635–650. [CrossRef]
72. Kroonenberg, S.B. Effects of provenance, sorting and weathering on the geochemistry of fluvial sands from different tectonic and climatic environments. In *Proceedings of the 29th International Geological, Part A*; VSP: Ultrecht, The Netherlands, 1994; pp. 69–81.
73. McLennan, S.M.; Taylor, S.R. Sedimentary rocks and crustal evolution: Tectonic setting and secular trends. *J. Geol.* **1991**, *99*, 1–21. [CrossRef]
74. Bauluz, B.; Mayayo, M.J.; Fernandez, N.C.; Lopez, J.M. Geochemistry of Precambrian and Paleozoic siliciclastic rocks from the Iberian Range (NE Spain): Implications for source-area weathering, sorting, provenance, and tectonic setting. *Chem. Geol.* **2000**, *168*, 135–150. [CrossRef]
75. Murali, A.V.; Parthasarathy, R.; Mahadevan, T.M.; Das, S.M. Trace element characteristics, REE patterns and partition coefficients of zircons from different geological environments: A case study on Indian zircons grains. *Geochim. Cosmochim. Acta* **1983**, *47*, 2047–2052. [CrossRef]

76. Barth, M.G.; McDonough, W.F.; Rudnick, R.L. Tracking the budget of Nb and Ta in the continental crust. *Chem. Geol.* **2000**, *165*, 197–213. [CrossRef]
77. Mo, X.X.; Pan, G.T. From the Tethys to the formation of the Qinghai-Tibet Plateau: Constrained by tectono-magmatic events. *Earth Sci. Front.* **2006**, *13*, 43–49.
78. Dickinson, W.R.; Gehrels, G.E. Use of U–Pb ages of detrital zircons to infer maximum depositional ages of strata: A test against a Colorado Plateau Mesozoic database. *Earth Planet. Sci. Lett.* **2009**, *288*, 115–125. [CrossRef]
79. Gehrels, G.; Kapp, P.; DeCelles, P.; Pullen, A.; Blakey, R.; Weislogel, A.; Ding, L.; Guynn, J.; Martin, A.; McQuarrie, N.; et al. Detrital zircon geochronology of pre-Tertiary strata in the Tibetan–Himalayan orogen. *Tectonics* **2011**, *30*, 1–27. [CrossRef]
80. Leier, A.; Kapp, P.; Gehrels, G.E.; DeCelles, P.G. Detrital zircon geochronology of Carboniferous-Cretaceous strata in the Lhasa terrane, Southern Tibet. *Basin Res.* **2007**, *19*, 361–378. [CrossRef]
81. Weislogel, A.L.; Graham, S.A.; Chang, E.Z.; Wooden, J.L.; Gehrels, G.E. Detrital zircon provenance from three turbidite depocenters of the Middle–Upper Triassic Songpan-Ganzi complex, central China: Record of collisional tectonics, erosional exhumation, and sediment production. *Geol. Soc. Am. Bull.* **2010**, *122*, 2041–2062. [CrossRef]
82. Zhao, X.F.; Zhou, M.F.; Li, J.W.; Sun, M.; Gao, J.F.; Sun, W.H.; Yang, J.S. Late Paleoproterozoic to early Mesoproterozoic Dongchuan Formation in Yunnan, SW China: Implications for tectonic evolution of the Yangtze Block. *Precambrian Res.* **2010**, *182*, 57–69. [CrossRef]
83. Lai, C.K. Tectonic Evolution of the Ailaoshan Fold Belt in Southwestern Yunnan, China. Ph.D. Thesis, University of Tasmania, Hobart, Australia, 2012.
84. Yang, J.; Cawood, P.A.; Du, Y.; Huang, H.; Hu, L. Detrital record of Indosinian mountain building in SW China: Provenance of the Middle Triassic turbidites in the Youjiang Basin. *Tectonophysics* **2012**, 105–117. [CrossRef]
85. DeCelles, P.G.; Gehrels, G.E.; Quade, J.; La, R.B.; Spurlin, M. Tectonic implications of U-Pb zircon ages of the Himalayan Orogenic Belt in Nepal. *Science* **2000**, *288*, 497–499. [CrossRef] [PubMed]
86. Cawood, P.A.; Johnson, M.W.; Nemchin, A.A. Early Palaeozoic orogenesis along the Indian margin of Gondwana: Tectonic response to Gondwana assembly. *Earth Planet. Sci. Lett.* **2007**, *255*, 70–84. [CrossRef]
87. Dong, C.Y.; Li, C.; Wan, Y.S.; Wang, W.; Wu, Y.W.; Xie, H.Q.; Liu, D.Y. Detrital zircon age model of Ordovician Wenquan quartzite south of Lungmuco-Shuanghu suture in the Qiangtang area, Tibet: Constraint on tectonic affinity and source regions. *Sci. China Earth Sci.* **2011**, *54*, 1034–1042. [CrossRef]
88. He, S.P.; Li, R.S.; Wang, C.; Zhang, H.F.; Ji, W.H.; Yu, P.S.; Gu, P.Y.; Shi, C. Discovery of ~4.0 Ga detrital zircons in the Changdu block, north Qiangtang, Tibetan Plateau. *Chin. Sci. Bull.* **2011**, *56*, 647–658. [CrossRef]
89. Tan, Y.; Bi, X.W.; Li, J.G.; Zhu, F.L.; Liao, M.Y.; Li, Y.B. Geochemistry and petrogenesis of the Jitang granitoids in Tibet, SW China. *Acta Petrol. Sin.* **2011**, *27*, 2763–2774.
90. Li, X.H.; Wang, C.S.; Yi, H.S.; Li, Y. Middle Cretacous and Eocene lithofacies and palegeography in Tibet. *Reg. Geol. China* **2001**, *20*, 82–88.
91. Vermeesch, P. How many grains are needed for a provenance study? *Earth Planet. Sci. Lett.* **2004**, *224*, 441–451. [CrossRef]
92. Fornelli, A.; Festa, V.; Micheletti, F.; Spiess, R.; Tursi, F. Building an Orogen: Review of U-Pb Zircon Ages from the Calabria–Peloritani Terrane to Constrain the Timing of the Southern Variscan Belt. *Minerals* **2020**, *10*, 944. [CrossRef]